A method for evaluating the transport and energy conversion properties of polymer biomembranes using the Kedem–Katchalsky–Peusner equations

Metoda oceny właściwości transportowych i konwersji energii w biomembranach polimerowych z wykorzystaniem równań Kedem–Katchalskiego–Peusnera

Andrzej Ślęzak[1,A,C–F], Sławomir Marek Grzegorczyn[2,C–F], Anna Pilis[1,B], Izabella Ślęzak-Prochazka[3,4,E,F]

[1] Faculty of Medicine and Health Science, Jan Dlugosz University, Częstochowa, Poland
[2] Department of Biophysics, Faculty of Medical Sciences in Zabrze, Medical University of Silesia, Poland
[3] Department of Systems Biology and Engineering, Silesian University of Technology, Gliwice, Poland
[4] Biotechnology Center, Silesian University of Technology, Gliwice, Poland

A – research concept and design; B – collection and/or assembly of data; C – data analysis and interpretation; D – writing the article; E – critical revision of the article; F – final approval of the article

Polymers in Medicine, ISSN 0370-0747 (print), ISSN 2451-2699 (online) *Polim Med*. 2023;53(1):25–36

Address for correspondence
Sławomir Marek Grzegorczyn
E-mail: grzegorczyn@sum.edu.pl

Funding sources
None declared

Conflict of interest
None declared

Received on November 29, 2022
Reviewed on February 16, 2023
Accepted on February 28, 2023

Published online on May 16, 2023

Cite as
Ślęzak A, Grzegorczyn SM, Pilis A, Ślęzak-Prochazka I. A method for evaluating the transport and energy conversion properties of polymer biomembranes using the Kedem–Katchalsky–Peusner equations. *Polim Med*. 2023;53(1):25–36. doi:10.17219/pim/161743

DOI
10.17219/pim/161743

Copyright
Copyright by Author(s)
This is an article distributed under the terms of the Creative Commons Attribution 3.0 Unported (CC BY 3.0) (https://creativecommons.org/licenses/by/3.0/)

Abstract

Background. A basic parameter in non-equilibrium thermodynamics is the production of entropy (*S*-entropy), which is a consequence of the irreversible processes of mass, charge, energy, and momentum transport in various systems. The product of *S*-entropy production and absolute temperature (*T*) is called the dissipation function and is a measure of energy dissipation in non-equilibrium processes.

Objectives. This study aimed to estimate energy conversion in membrane transport processes of homogeneous non-electrolyte solutions. The stimulus version of the *R*, *L*, *H*, and *P* equations for the intensity of the entropy source achieved this purpose.

Materials and methods. The transport parameters for aqueous glucose solutions through Nephrophan® and Ultra-Flo 145 dialyser® synthetic polymer biomembranes were experimentally determined. Kedem–Katchalsky–Peusner (KKP) formalism was used for binary solutions of non-electrolytes, with Peusner coefficients introduced.

Results. The *R*, *L*, *H*, and *P* versions of the equations for the *S*-energy dissipation were derived for the membrane systems based on the linear non-equilibrium Onsager and Peusner network thermodynamics. Using the equations for the *S*-energy and the energy conversion efficiency factor, equations for *F*-energy and *U*-energy were derived. The *S*-energy, *F*-energy and *U*-energy were calculated as functions of osmotic pressure difference using the equations obtained and presented as suitable graphs.

Conclusions. The *R*, *L*, *H*, and *P* versions of the equations describing the dissipation function had the form of second-degree equations. Meanwhile, the *S*-energy characteristics had the form of second-degree curves located in the 1st and 2nd quadrants of the coordinate system. These findings indicate that the *R*, *L*, *H*, and *P* versions of *S*-energy, *F*-energy and *U*-energy are not equivalent for the Nephrophan® and Ultra-Flo 145 dialyser® membranes.

Keywords: membrane transport, Kedem–Katchalsky–Peusner equations, polymer biomembrane, transport coefficients, *S*-entropy production

Streszczenie

Wprowadzenie. Podstawowym parametrem termodynamiki nierównowagowej jest produkcja *S*-entropii, która jest konsekwencją nieodwracalnych procesów transportu masy, ładunku, energii i pędu w różnych typach układów. Iloczyn produkcji *S*-entropii i temperatury bezwzględnej *T* nazywany jest funkcją rozpraszania i jest miarą rozpraszania energii w procesach nierównowagowych.

Cel pracy. Celem pracy było oszacowanie konwersji energii w procesach transportu membranowego jednorodnych roztworów nieelektrolitów. W tym celu wykorzystano bodźcową wersję równań *R*, *L*, *H* i *P* dla natężenia źródła entropii.

Materiał i metody. Przedmiotem badań były syntetyczne biomembrany polimerowe (Nephrophan® i Ultra-Flo 145 dialyser®) o eksperymentalnie wyznaczonych parametrach transportu dla wodnych roztworów glukozy. Jako metodę badawczą zastosowano formalizm Kedem–Katchalsky'ego–Peusnera dla binarnych roztworów nieelektrolitów, z wprowadzonymi współczynnikami Peusnera.

Wyniki. Wersje *R*, *L*, *H* i *P* równań dyssypacji *S*-energii zostały wyprowadzone dla układu membranowego na podstawie liniowej nierównowagowej termodynamiki sieciowej Onsagera i Peusnera. Korzystając z równania na *S*-energię i równania na współczynnik sprawności konwersji energii, wyprowadzono równania na *F*-energię i *U*-energię. Na podstawie otrzymanych równań obliczono *S*-energię, *F*-energię i *U*-energię jako funkcje różnicy ciśnień osmotycznych i przedstawiono je w postaci odpowiednich wykresów.

Wnioski. Wersje *R*, *L*, *H* i *P* równań opisujących funkcję dyssypacji mają postać równań drugiego stopnia. Charakterystyki *S*-energii mają postać krzywych drugiego stopnia znajdujących się w pierwszej i drugiej ćwiartce układu współrzędnych. Artykuł pokazuje, że wersje *R*, *L*, *H* i *P* *S*-energii, *F*-energii i *U*-energii nie są równoważne zarówno dla membran Nephrophan®, jak i Ultra-Flo 145 dialyser®.

Słowa kluczowe: transport membranowy, biomembrana polimerowa, współczynniki transportu, produkcja *S*-entropii, równania Kedem–Katchalsky'ego–Peusnera

Background

Thermodynamic entropy (*S*-entropy) is the only physical parameter that indicates the irreversible one-way time course of biological processes.[1] An increase in *S*-entropy results from the transition from a more to a less ordered state that is less precisely understood than the initial state. For this reason, the applicability of the concept of *S*-entropy is limited to linear irreversible processes in states close to equilibrium.[2] Nevertheless, it plays an important role in the study of non-equilibrium processes by quantitatively characterizing the degree of irreversibility of physicochemical processes, including biological ones, that fulfill the second law of thermodynamics expressed as the law of increase of entropy.[3–6]

One of the basic parameters in non-equilibrium thermodynamics is the production of *S*-entropy, which is a consequence of irreversible processes of mass, charge, energy, and momentum transport in various systems, including membrane systems.[7,8] Membrane transport processes are important in many areas of human cognitive and utilitarian activity, including science, technology and medicine.[9] Research methods and tools developed using non-equilibrium thermodynamics and network thermodynamics describe such membrane transport,[5,10] including the Kedem–Katchalsky[5] and Kedem–Katchalsky–Peusner[10–16] formalisms. Several papers[5,7,8,13,17] focused on estimating the entropy source in membrane systems used equations derived from the Kedem–Katchalsky formalism, while others presented entropy calculations for bacterial nanocellulose and Textus Bioactiv biomembranes used as active dressings.[18–20] The product of *S*-entropy production and absolute temperature (*T*) is termed the dissipation function and is a measure of energy dissipation in non-equilibrium processes.

The present work aimed to evaluate the energy conversion in membrane systems using the formalism developed within the framework of Peusner network thermodynamics. The introduction presents the equations for *S*-energy dissipation in the Kedem and Katchalsky versions, the *R*, *L*, *H*, and *P* versions of the Kedem–Katchalsky–Peusner (KKP) equations for membrane transport of homogeneous non-electrolyte solutions, the equations representing the *R*, *L*, *H*, and *P* versions of the *Q* coupling parameter, and the energy conversion efficiency ratio. This part also contains the mathematical equations for $\phi(S)_{Y\,(Y=\mathrm{R},L,H\text{ or }P)}$, derived from the KKP formalism describing the energy dissipation function as a function of thermodynamic forces. Based on the obtained equations $R_{ij} = f(\Delta\pi)_{\Delta P\,=\,0}$, $L_{ij} = f(\Delta\pi)_{\Delta P\,=\,0}$, $H_{ij} = f(\Delta\pi)_{\Delta P\,=\,0,}$ and $P_{ij} = f(\Delta\pi)_{\Delta\pi\,=\,0}$ $(i,j \in \{1, 2\})$, the characteristics of $\phi(S)_{Y\,(Y=\mathrm{R},L,H\text{ or }P)} = f(\Delta\pi)_{\Delta\pi\,=\,0}$ were calculated for Ultra-Flo 145 dialyser® and Nephrophan® synthetic membranes. To evaluate the conversion of chemical energy, the value of the coupling parameter and the energy conversion efficiency was calculated.

Materials and methods

Membrane system

The system used to study membrane transport is illustrated schematically in Fig. 1. This system consists of a membrane located in the horizontal plane that separates 2 aqueous solutions of glucose with initial concentrations

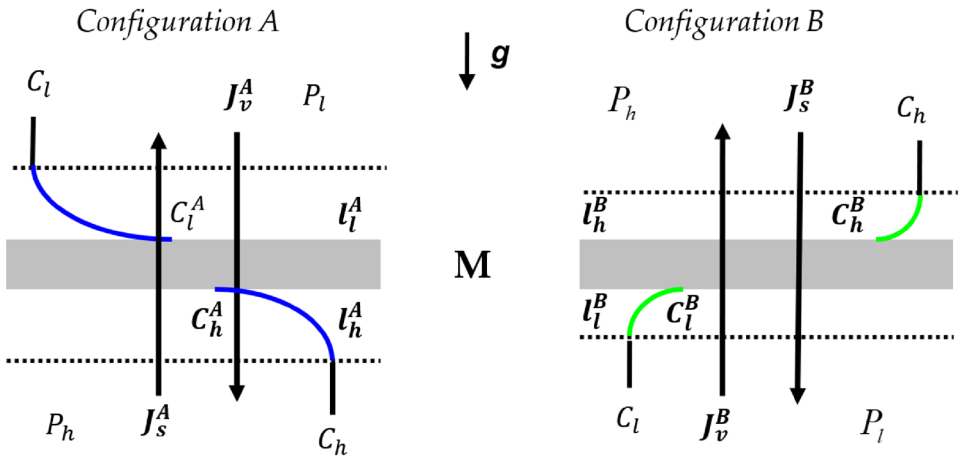

Fig. 1. Model of a single-membrane system

M – membrane; g – gravitational acceleration; l_l^A and l_h^A – concentration boundary layers (CBLs) in configuration A; l_l^B and l_h^B – CBLs in configuration B; P_h and P_l – mechanical pressures; C_h and C_l – total solution concentrations ($C_h > C_l$); C_l^A, C_h^A, C_l^B and C_h^B – local (at boundaries between membrane and CBLs) solution concentrations; J_v^A – solute and volume fluxes in configuration A; J_v^B – solute and volume fluxes in configuration B.

of C_h and C_l = const. ($C_h \geq C_l$). The density of solutions with concentrations of C_h and C_l fulfilled the condition $\rho_h \geq \rho_l$ (ρ_l = const.). In configuration A, the compartment above the membrane contains a solution with concentration C_l, and the compartment below the membrane has a solution with the concentration C_h. In configuration B, the solutions with the concentration of C_l and C_h were reversed.

Water and dissolved substances transported through the membrane cause membrane concentration polarization (CP) since they form concentration boundary layers (CBLs), l_h^r and l_l^r, on both sides of the membrane. The thickness of the CBL (l_h^r) is δ_h^r, and the thickness of CBL (l_l^r) is δ_l^r. As a consequence of the CBL formation, the concentration difference through the membrane decreases from $C_h - C_l$ to $C_h^r - C_l^r$, where $C_h^r > C_l^r$ $C_h > C_h^r$, and $C_l^r > C_l$, and the density difference increases from $\rho_h - \rho_l$ to $\rho_h^r - \rho_l^r$, where $\rho_h^r > \rho_l^r$, $\rho_h > \rho_h^r$, and $\rho_l^r > \rho_l$. When a lower-density solution is located in the compartment below the membrane, and a higher-density solution is in the compartment above the membrane, the complex l_h^r/M/l_l^r, can lose hydrodynamic stability.

Hydrodynamic instability is manifested by natural convection in near-membrane areas.[21–23] When the concentration Rayleigh number (R_C), which provides information about the process of the appearance of gravitational convection, exceeds its critical value, hydrodynamic instabilities appear in the near membrane areas.[13,22,24–26] Over time, the destructive effect of gravitational convection limits the growth of δ_h^r and δ_l^r, and accelerates the diffusion of substances beyond the layers, which extends the convection to the entire volume of the solution. Self-organization of the liquid may occur under certain conditions, which is manifested in the "plum structure."[27]

Equations for *S*-energy dissipation in the Kedem–Katchalsky version

The measure of *S*-energy dissipation is the so-called dissipation function $\phi(S)$, which is equal to the product of T and entropy production (d_iS/dt). Mathematical expressions for *S*-energy dissipation in a system in which a membrane separates 2 homogeneous non-electrolytic solutions of different concentrations will be obtained using the procedure described in previous papers.[3,5] The *S*-energy dissipation function can be described by the expression (Eq. 1):

$$\phi(S) = T\frac{d_iS}{dt} = \sum_{i=1}^{n} J_i X_i = \sum_{i=1}^{n} L_{ii} X_i^2 + \sum_{i,j(i\neq j)=1}^{n} (L_{ij} + L_{ji}) X_i X_j \geq 0 \quad (1)$$

This equation shows that $\phi(S)$ is a bilinear form and is the sum of the products of the generalized thermodynamic fluxes (J_i) and the thermodynamic forces (X_i) of the same tensor order. In this equation, L_{ij} are phenomenological coefficients coupling J_i with X_j.[5] Diagonal (L_{ii}, L_{jj}) and non-diagonal (L_{ij}, L_{ji}) coefficients satisfy the following Onsager relations:

$$L_{ij} \neq L_{ji},\ L_{ii} \geq 0,\ L_{jj} \geq 0,\ L_{ii}L_{jj} \geq L_{ij}^2\ (i,j \in \{1, 2\})^{3,5}$$

For stationary membrane transport of homogeneous non-electrolytic solutions containing 1 solute (s) and solvent (w), caused by thermodynamic forces, $\Delta\pi$ (osmotic pressure difference) and ΔP (hydrostatic pressure difference), the Equation (1) can be written in the form (Eq. 2)[5]:

$$\phi(S)_{Y\,(Y=R,L,H,\text{ or }P)} = J_w\bar{V}_w(\Delta P - \Delta\pi) + J_s\left(\bar{V}_s\Delta P + \frac{\Delta\pi}{\bar{C}_s}\right) \quad (2)$$

where $\bar{V}_s$ and $\bar{V}_w$ denote the partial molar volumes of the s-th and w-th component of the solution, J_s and J_w are the fluxes of s and w, respectively, $\bar{C}_s = (C_h - C_l)\ln(C_hC_l^{-1})]^{-1}$, C_h and C_l ($C_h > C_l$) are solute concentrations, $\Delta\pi = RT(C_h - C_l)$ is the osmotic pressure difference, and RT is the product of the gas constant and absolute temperature. $\bar{C}_s$ can also be expressed as $\bar{C}_s = \Delta\pi[RT\ln(C_hC_l^{-1})]^{-1}$.

Taking into consideration the expressions $J_s\bar{V}_s + J_w\bar{V}_w \equiv J_v$ and $J_s\bar{C}_s^{-1} - J_w\bar{V}_w \equiv J_D$ (J_v – volume flux, J_D – diffusive flux), we can write Equation (2) in the form (Eq. 3)[3,5]:

$$\phi(S)_{Y\,(Y=R,L,H,\text{ or }P)} = J_v(\Delta P - \Delta\pi) + J_s\left(\frac{1}{\bar{C}_s} + \bar{V}_s\right)\Delta\pi \quad (3)$$

Assuming glucose concentration C_h = 201 mol m^{-3} and C_l = 1 mol m^{-3}, we get $\bar{C}_s$ = 37.71 mol m^{-3} and $1/\bar{C}_s = 2.65 \times 10^{-2}$ m^3 mol^{-1}. On the other hand, $\bar{V}_s = 1.2 \times 10^{-4}$ m^3 mol^{-1}.

This means that $1/\bar{C}_s >> \bar{V}_s$, and Equation (3) can be written in the form (Eq. 4):

$$\phi(S)_{Y\,(Y=R,L,H,\text{ or }P)} = J_v(\Delta P - \Delta\pi) + J_s\frac{\Delta\pi}{\bar{C}_S} \tag{4}$$

The expression obtained is a practical form of the *S*-energy dissipation function for the osmotic-diffusion transport of homogeneous solutions. The $\phi(S)_{Y\,(Y=R,L,H\text{ or }P)}$ of Equation (3) can then be written using the *R*, *L*, *H*, and *P* versions of the KKP equations.

R, *L*, *H*, and *P* versions of the Kedem–Katchalsky–Peusner equations

The *R*, *L*, *H*, and *P* versions of the KKP equations are obtained through an appropriate transformation of the classical Kedem–Katchalsky equations (Eq. 5,6),[5]

$$J_v = L_p\Delta P - L_p\sigma\Delta\pi \tag{5}$$

$$J_s = \omega\Delta\pi + \bar{C}_s(1-\sigma)J_v \tag{6}$$

where L_p, σ, and ω are coefficients of hydraulic permeability and reflection and diffusion permeability, respectively, J_v is volume flux, J_s is solute flux, ΔP is the hydrostatic pressure difference, $\Delta\pi = RT\Delta C$ is the osmotic pressure difference, RT is the product of the gas constant and absolute temperature, $\Delta C = C_h - C_l$ ($C_h > C_l$) is the difference of concentrations on the membrane, and $\bar{C}_s = (C_h - C_l)[\ln(C_hC_l^{-1})]^{-1} = \Delta\pi[RT\ln(C_hC_l^{-1})]^{-1}$ is the average concentration of the solution in the membrane.

By appropriate transformations of Equations (5) and (6), it is possible to obtain the *R*, *L*, *H*, and *P* versions of the KKP equations.[10,14] The *R*, *L*, *H*, and *P* versions of the KKP equations obtained as a result of the transformation of Equations (5) and (6) are summarized in Table 1. The *R*, *L*, *H*, and *P* versions of the KKP equations contain Peusner coefficients, R_{ij}, L_{ij}, H_{ij}, and P_{ij}, where $i, j \in \{1, 2\}$, respectively.

R, *L*, *H*, and *P* versions of the *Q* coupling parameter and energy conversion ratio e_{max}

Using the definition of the *Q* coupling parameter and the energy conversion efficiency, $(e_{max})_{Y\,(Y=R,L,H\text{ or }P)}$, presented by Peusner,[10] expressions for the *R*, *L*, *H*, and *P* versions of the *Q* coupling parameter and $(e_{max})_{Y\,(Y=R,L,H\text{ or }P)}$ coefficients can be written. These expressions are listed in the 2nd and 3rd columns of Table 2.

Taking into account the equations listed in the 2nd, 3rd and 4th columns of Table 2, and the expressions listed in the 3rd column of Table 1, we get (Eq. 7–9):

$$r_{12} = l_{12} = \frac{L_p(1-\sigma)^2\Delta\pi}{\omega RT\ln\frac{C_h}{C_l} + L_p(1-\sigma)^2\Delta\pi} = r_{21} = l_{21} \tag{7}$$

$$h_{12} = p_{12} = \frac{L_p(1-\sigma)^2\Delta\pi}{\omega RT\ln\frac{C_h}{C_l}} = -h_{21} = -p_{21} \tag{8}$$

$$Q_R = Q_L = \frac{L_p(1-\sigma)^2\Delta\pi}{\omega RT\ln\frac{C_h}{C_l} + L_p(1-\sigma)^2\Delta\pi} = -Q_H = -Q_P \tag{9}$$

R, *L*, *H*, and *P* versions of the equation for energy dissipation

Taking into account the *R*, *L*, *H*, and *P* versions of the KKP equations in Equation (3), we obtain the *R*, *L*, *H*, and *P* versions of the *S*-energy dissipation equations for the thermodynamic force version denoted by $\phi(S)_R$, $\phi(S)_L$, $\phi(S)_H$, and $\phi(S)_P$ (Eq. 10–13):

$$\phi(S)_R = \frac{1}{(R_{11}R_{22} - R_{12}R_{21})}\left[R_{22}(\Delta P - \Delta\pi)^2 - (R_{12} + R_{21})(\Delta P - \Delta\pi)\frac{\Delta\pi}{\bar{C}_S} + R_{11}\left(\frac{\Delta\pi}{\bar{C}_S}\right)^2\right] \tag{10}$$

$$\phi(S)_L = L_{11}(\Delta P - \Delta\pi)^2 + (L_{12} + L_{21})(\Delta P - \Delta\pi)\frac{\Delta\pi}{\bar{C}_S} + L_{22}\left(\frac{\Delta\pi}{\bar{C}_S}\right)^2 \tag{11}$$

$$\phi(S)_H = \frac{1}{H_{11}}\left[(\Delta P - \Delta\pi)^2 + (H_{21} - H_{12})(\Delta P - \Delta\pi)\frac{\Delta\pi}{\bar{C}_S} + (H_{11}H_{22} - H_{12}H_{12})\left(\frac{\Delta\pi}{\bar{C}_S}\right)^2\right] \tag{12}$$

$$\phi(S)_P = \frac{1}{P_{22}}\left[(P_{11}P_{22} - P_{12}P_{21})(\Delta P - \Delta\pi)^2 + (P_{12} - P_{21})(\Delta P - \Delta\pi)\frac{\Delta\pi}{\bar{C}_S} + \left(\frac{\Delta\pi}{\bar{C}_S}\right)^2\right] \tag{13}$$

These equations do not contain J_v and J_s fluxes, but do contain the thermodynamic forces ΔP and $\Delta\pi$. Therefore, these equations determine the thermodynamic forces of the equations for $\phi(S)_{Y\,(Y=R,L,H\text{ or }P)}$. From Equations (10–13), it follows that in order to calculate $\phi(S)_{Y\,(Y=R,L,H\text{ or }P)}$, the characteristics $R_{ij} = f(\Delta\pi)_{\Delta P=0}$, $L_{ij} = f(\Delta\pi)_{\Delta P=0}$, $H_{ij} = f(\Delta\pi)_{\Delta P=0}$, and $P_{ij} = f(\Delta\pi)_{\Delta P=0}$ must first be calculated and included in Equations (7–9).

Evaluation of internal energy conversion

The internal energy conversion process is governed by the principle of conservation of energy. According to this principle, the fluxes of the *U*-energy ($\phi(U)_{Y\,(Y=R,L,H\text{ or }P)}$), *F*-energy ($\phi(F)_{Y\,(Y=R,L,H\text{ or }P)}$) and *S*-energy ($\phi(S)_{Y\,(Y=R,L,H\text{ or }P)}$) satisfy the equation (Eq. 14)[28]:

$$\phi(U)_{Y\,(Y=R,L,H,\text{ or }P)} = \phi(F)_{Y\,(Y=R,L,H,\text{ or }P)} = \phi(S)_{Y\,(Y=R,L,H,\text{ or }P)} \tag{14}$$

Table 1. Comparison of the *R*, *L*, *H*, and *P* versions of the Kedem–Katchalsky–Peusner (KKP) equations

KKP version	Form of the equations	Peusner's coefficients
R	$\Delta P - \Delta\pi = R_{11}J_v + R_{12}J_s$ $\frac{\Delta\pi}{\bar{C}_s} = R_{11}J_v + R_{12}J_s$	$R_{11} = \frac{\omega RT \ln\frac{C_h}{C_l} + \Delta\pi(1-\sigma)^2 L_p}{L_p \omega RT \ln\frac{C_h}{C_l}}$ $R_{12} = -\frac{1-\sigma}{\omega} = R_{21}$ $R_{22} = \frac{RT \ln\frac{C_h}{C_l}}{\omega\Delta\pi}$
L	$J_v = L_{11}(\Delta P - \Delta\pi) + L_{12}\frac{\Delta\pi}{\bar{C}_s}$ $J_s = L_{21}(\Delta P - \Delta\pi) + L_{22}\frac{\Delta\pi}{\bar{C}_s}$	$L_{11} = L_p$ $L_{12} = \frac{\Delta\pi}{RT \ln\frac{C_h}{C_l}}(1-\sigma)L_p = L_{21}$ $L_{22} = \frac{\Delta\pi}{RT \ln\frac{C_h}{C_l}}\left(\omega + \frac{\Delta\pi(1-\sigma)^2 L_p}{RT \ln\frac{C_h}{C_l}}\right)$
H	$\Delta P - \Delta\pi = H_{11}J_v + L_{12}\frac{\Delta\pi}{\bar{C}_s}$ $J_s = H_{21}J_v + H_{22}\frac{\Delta\pi}{\bar{C}_s}$	$H_{11} = \frac{1}{L_p}$ $H_{12} = \frac{\Delta\pi}{RT \ln\frac{C_h}{C_l}}(1-\sigma) = -H_{21}$ $H_{22} = \frac{\omega\Delta\pi}{RT \ln\frac{C_h}{C_l}}$
P	$J_v = P_{11}(\Delta P - \Delta\pi) + P_{12}J_s$ $\frac{\Delta\pi}{\bar{C}_s} = P_{21}(\Delta P - \Delta\pi) + P_{22}J_s$	$P_{11} = \frac{L_p \omega RT \ln\frac{C_h}{C_l}}{\omega RT \ln\frac{C_h}{C_l} + \Delta\pi(1-\sigma)^2 L_p}$ $P_{12} = \frac{(1-\sigma)L_p \omega RT \ln\frac{C_h}{C_l}}{\omega RT \ln\frac{C_h}{C_l} + \Delta\pi(1-\sigma)^2 L_p} = -P_{21}$ $P_{22} = \frac{\left(\omega RT \ln\frac{C_h}{C_l}\right)^2}{\left(\omega RT \ln\frac{C_h}{C_l} + \Delta\pi(1-\sigma)^2 L_p\right)\Delta\pi}$

Here, $\phi(U)_Y = A^{-1}dU_Y/dt$ is the *U*-energy flux (W m^{-2}), $\phi(F)_Y = A^{-1}dF_Y/dt$ the *F*-energy flux (W m^{-2}), and $\phi(S)_Y = TA^{-1}d_iS_Y/dt$ is the *S*-energy flux (W m^{-2}).

An explicit form of the coefficients R_{ij}, L_{ij}, H_{ij}, and P_{ij}, for $i,j \in \{1, 2\}$, appearing in the above equation is given in Equations (10–13). To obtain *S*-energy for the conditions of homogeneity of solutions ($\phi(S)_{Y(Y=\mathrm{R},L,H\,\mathrm{or}\,P)}$) in Equations (10–13), the free energy flux $\phi(F)_{Y(Y=\mathrm{R},L,H\,\mathrm{or}\,P)}$ can be calculated using the definition of the energy conversion efficiency coefficient (Eq. 15):

$$(e_{\max})_{Y(Y=R,L,H,\text{ or }P)} = \frac{\phi(F)_{Y(Y=R,L,H,\text{ or }P)}}{\phi(U)_{Y(Y=R,L,H,\text{ or }P)}} = \frac{\phi(F)_{Y(Y=R,L,H,\text{ or }P)}}{\phi(U)_{Y(Y=R,L,H,\text{ or }P)} + \phi(U)_{Y(Y=R,L,H,\text{ or }P)}} \quad (15)$$

By transforming Equation (15), we get (Eq. 16,17)

$$\phi(F)_{Y(Y=R,L,H,\text{ or }P)} = \frac{(e_{\max})_{Y(Y=R,L,H,\text{ or }P)}}{1-(e_{\max})_{Y(Y=R,L,H,\text{ or }P)}}\phi(S)_{Y(Y=R,L,H,\text{ or }P)} \quad (16)$$

$$\phi(U)_{Y(Y=R,L,H,\text{ or }P)} = \frac{1}{1-(e_{\max})_{Y(Y=R,L,H,\text{ or }P)}}\phi(S)_{Y(Y=R,L,H,\text{ or }P)} \quad (17)$$

From a formal point of view, the cases of $\phi(F)_{Y(Y=\mathrm{R},L,H\,\mathrm{or}\,P)} = 0$ and $\phi(U)_{Y(Y=\mathrm{R},L,H\,\mathrm{or}\,P)} = 0$ are excluded, because in order for the denominator of Equations (16) and (17) to be different from 0, the condition $(e_{max})_{Y(Y=\mathrm{R},L,H\,\mathrm{or}\,P)} \neq 1$ must be satisfied.

The maximum energy conversion efficiency expressed by the Kedem–Caplan–Peusner coefficients[10,28,29] in Equations (16) and (17) can be written as (Eq. 18–21):

Table 2. *R*, *L*, *H*, and *P* versions of coupling coefficient *l*, coupling parameter *Q* and energy conversion coefficient $(e_{max})_{Y\,(Y=R,L,H\text{ or }P)}$

Version	Caplan coupling parameter	Peusner coupling parameter	Energy conversion coefficient
R	$r_{12} = \frac{-R_{12}}{\sqrt{R_{11}R_{22}}}$	$Q_R = \frac{2\lvert R_{21}R_{12}\rvert}{4R_{11}R_{22} - 2R_{21}R_{12}}$	$(e_{\max})_R = \frac{\frac{R_{21}}{R_{12}}Q_R}{1 + \sqrt{1-Q_R^2}}$
L	$l_{12} = \frac{L_{12}}{\sqrt{L_{11}L_{22}}}$	$Q_L = \frac{2\lvert L_{21}L_{12}\rvert}{4L_{11}L_{22} - 2L_{21}L_{12}}$	$(e_{\max})_L = \frac{\frac{L_{21}}{L_{12}}Q_L}{1 + \sqrt{1-Q_L^2}}$
H	$h_{12} = \frac{H_{12}}{\sqrt{H_{11}H_{22}}}$	$Q_H = \frac{2\lvert H_{21}H_{12}\rvert}{4H_{11}H_{22} - 2H_{21}H_{12}}$	$(e_{\max})_H = \frac{\frac{H_{21}}{H_{12}}Q_H}{1 + \sqrt{1-Q_H^2}}$
P	$p_{12} = \frac{-P_{12}}{\sqrt{P_{11}P_{22}}}$	$Q_P = \frac{2\lvert P_{21}P_{12}\rvert}{4P_{11}P_{22} - 2P_{21}P_{12}}$	$(e_{\max})_P = \frac{\frac{P_{21}}{P_{12}}Q_P}{1 + \sqrt{1-Q_P^2}}$

$$(e_{\max})_R = (e_{\max})_r = \frac{R_{12}R_{21}}{R_{11}R_{22}\left(1 + \sqrt{1-\frac{R_{12}R_{21}}{R_{11}R_{22}}}\right)^2} = \frac{r_{12}r_{21}}{\left(1 + \sqrt{1-r_{12}r_{21}}\right)^2} \tag{18}$$

$$(e_{\max})_L = (e_{\max})_l = \frac{L_{12}L_{21}}{L_{11}L_{22}\left(1 + \sqrt{1-\frac{L_{12}L_{21}}{L_{11}L_{22}}}\right)^2} = \frac{l_{12}l_{21}}{\left(1 + \sqrt{1-l_{12}l_{21}}\right)^2} \tag{19}$$

$$(e_{\max})_H = (e_{\max})_h = \frac{H_{12}H_{21}}{H_{11}H_{22}\left(1 + \sqrt{1-\frac{H_{12}H_{21}}{H_{11}H_{22}}}\right)^2} = \frac{h_{12}h_{21}}{\left(1 + \sqrt{1-h_{12}h_{21}}\right)^2} \tag{20}$$

$$(e_{\max})_P = (e_{\max})_p = \frac{P_{12}P_{21}}{P_{11}P_{22}\left(1 + \sqrt{1-\frac{P_{12}P_{21}}{P_{11}P_{22}}}\right)^2} = \frac{p_{12}p_{21}}{\left(1 + \sqrt{1-p_{12}p_{21}}\right)^2} \tag{21}$$

The values of the $(e_{max})_{Y\,(Y=R,L,H\text{ or }P)}$ coefficient are limited by the relations $0 \le (e_{max})_{Y\,(Y=R,L,H\text{ or }P)} \le 1$ and $(e_{max})_{Y\,(Y=R,L,H\text{ or }P)} = 0$, when $R_{12}R_{21} = L_{12}L_{21} = H_{12}H_{21} = P_{12}P_{21} = 0$, when $r_{12}r_{21} = l_{12}l_{21} = h_{12}h_{21} = p_{12}p_{21} = 0$ and $(e_{max})_{Y\,(Y=R,L,H\text{ or }P)} = 1$, when $R_{12}R_{21} = R_{11}R_{22}$, $L_{12}L_{21} = L_{11}L_{22}$, $H_{12}H_{21} = H_{11}H_{22}$, or when $P_{12}P_{21} = P_{11}P_{22}$ and $r_{12}r_{21} = 1$, $l_{12}l_{21} = 1$, $h_{12}h_{21} = 1$ or $p_{12}p_{21} = 1$.

Biomembrane characteristics

Nephrophan® biomembrane (ORWO VEB Filmfabrik, Wolfen, Germany) is a microporous, highly hydrophilic, electroneutral, and compact-structure membrane made from regenerated cellulose.[30] The membrane is used in urology in ganglion hemodialyzers, due to their high-pressure strength, and for controlled release of drugs in ophthalmology and laryngology.[31]

The Ultra-Flo 145 dialyser® (Artificial Organs Division, Travenol Laboratories, Brussels, Belgium) is an ultrafiltration, microporous, hydrophilic, and electroneutral regenerated cellulose biomembrane used in urology.[32]

Images of Nephrophan® and Ultra-Flo 145 dialyser® membranes obtained with a Zeiss Supra 35 scanning electron microscope (SEM; Carl Zeiss AG, Jena, Germany) are shown in Fig. 2A,B. The image in Fig. 2A shows the solid structure of the Nephrophan® membrane, and the image in Fig. 2B presents the microfiber structure of the Ultra-Flo 145 dialyser® membrane.

Results

The calculations of $(\phi(S)_{Y\,(Y=R,L,H\text{ or }P)}$ performed for Nephrophan® and Ultra-Flo 145 dialyser® membranes have been used in nephrology and ophthalmology.[17] Each of the biomembranes (monolayer, symmetric, isotropic, and electrically neutral) separated 2 homogeneous aqueous glucose solutions with concentrations C_h and C_l ($C_h > C_l$) and the same temperature ($T = 295$ K). The transport properties of these biomembranes were determined by hydraulic permeability (L_p), reflection (σ) and diffusion permeability (ω). The dry thickness of the membranes

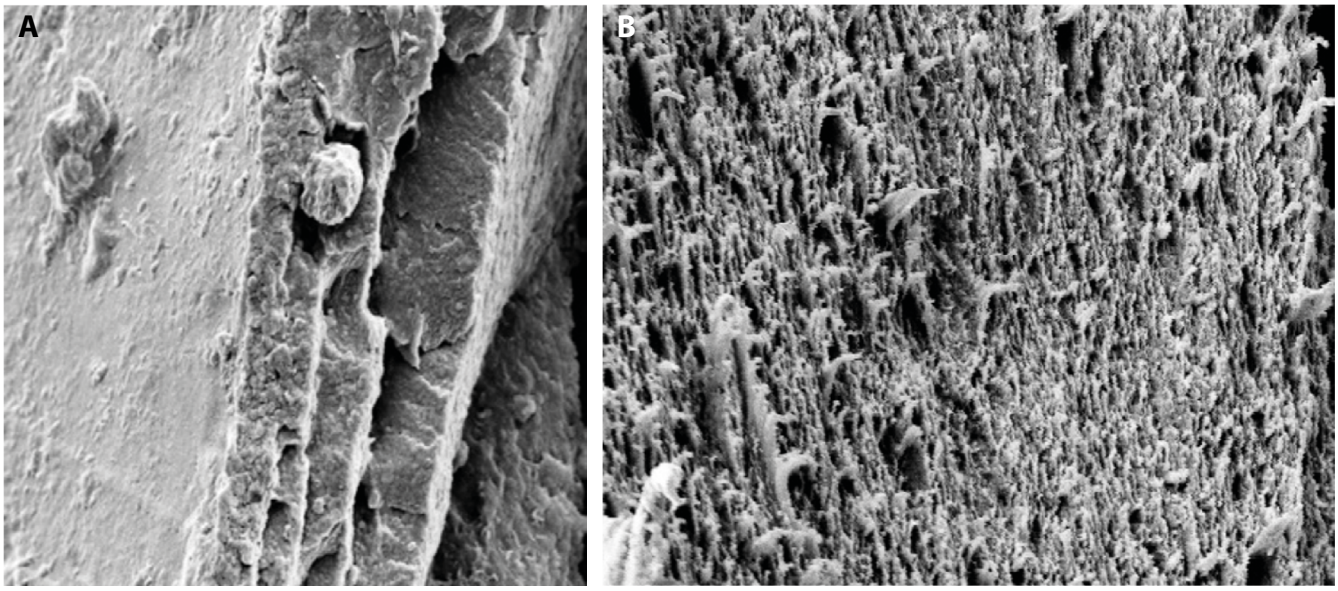

Fig. 2. Images of membrane surfaces obtained from scanning electron microscopy (SEM). A. Surface and cross-section of the Nephrophan® membrane (×15,000 magnification)[24]; B. Cross-section of the Ultra-Flo 145 dialyser® membrane (×10,500 magnification)

Table 3. Values of the parameters (L_p, σ, ω, and d) for Nephrophan® and Ultra-Flo 145 dialyser® membranes, and for aqueous glucose solutions

Parameters	Biomembrane	
	Nephrophan®	Ultra-Flo 145 dialyser®
$L_p \times 10^{12}$ [$m^3N^{-1}s^{-1}$]	4.9	0.85
σ	0.068	0.112
$\omega \times 10^9$ [mol $N^{-1}s^{-1}$]	0.8	0.1
d [μm]	200	800

is denoted by d. The values of these coefficients are summarized in Table 3.

Table 3 shows that both Nephrophan® and Ultra-Flo 145 dialyser® biomembranes are selective for glucose because $0 < \sigma < 1$. The following data was used for the calculations: $R = 8.31$ J $mol^{-1}K^{-1}$ and $\Delta\pi$, which ranged from –12.16 kPa to –502.54 kPa or from +12.16 kPa to +502.54 kPa, $C_l = 1$ mol m^{-3} and C_h ranged from 6 mol m^{-3} to 206 mol m^{-3}. To calculate the dependencies $R_{ij} = f(\Delta\pi)_{\Delta P=0}$, $L_{ij} = f(\Delta\pi)_{\Delta P=0}$, $H_{ij} = f(\Delta\pi)_{\Delta P=0}$, and $P_{ij} = f(\Delta\pi)_{\Delta P=0}$ ($i,j \in \{1, 2\}$), the equations listed in the 3rd column of Table 1 were used. All calculations assumed the condition ΔP = 0. The results of the calculations are presented in Fig. 3A–D, Fig. 4A–D and Fig. 5A. The results of calculations show that the values of the coefficients $R_{12} = R_{21}$, L_{11}, and H_{11} are independent of $\Delta\pi$. Therefore, their values are constant and amount to: $R_{12} = R_{21} = -1.165 \times 10^9$ N s mol^{-1}, $L_{11} = 4.9 \times 10^{-12}$ m^3 $N^{-1}s^{-1}$ and $H_{11} = 2.0 \times 10^{11}$ Ns m^{-3} for the Nephrophan® membrane, and $R_{12} = R_{21} = -8.88 \times 10^9$ N s mol^{-1}, $L_{11} = 0.85 \times 10^{-12}$ m^3 $N^{-1}s^{-1}$ and $H_{11} = 11.76 \times 10^{11}$ Ns m^{-3} for the Ultra-Flo 145 dialyser® membrane.

Increases in the absolute values of glucose osmotic pressure ($\Delta\pi$) cause a nonlinear increase of L_{12}, L_{21}, L_{22}, and R_{11} coefficients in all configurations of the system, while R_{22} decreases with increased absolute values of $\Delta\pi$. Greater changes of all the coefficients occurred for the Nephrophan® membrane than the Ultra-Flo 145 dialyser® membrane for the same changes in $\Delta\pi$. The smaller changes in coefficients for the Ultra-Flo 145 dialyser® membrane are related to its more porous structure, which makes it easier for solutes and water to permeate the membrane. Therefore, an increase in absolute values of $\Delta\pi$ causes greater coupling between suitable fluxes and forces, when the direct relationship between thermodynamic force and flux of glucose is excluded.

The values of coefficients R_{11}, R_{22}, L_{12}, L_{22}, H_{12}, H_{21}, H_{22}, P_{11}, P_{12}, and P_{22} depend on $\Delta\pi$ for both biomembranes, as is illustrated in Fig. 3A–D and Fig. 4A–D. Figure 3A,C,D and Fig. 4B show that the values of R_{11}, L_{12}, L_{22}, and H_{22} are positive and increase with increasing absolute $\Delta\pi$. Meanwhile, Fig. 3B and Fig. 4D,E demonstrate positive values of R_{22}, P_{11}, P_{12}, and P_{22}, which decrease with increasing absolute $\Delta\pi$. In turn, H_{12} and P_{21} are negative, and H_{12} decreases, while the values of P_{21} increase with increasing absolute $\Delta\pi$. Furthermore, Fig. 3A–D and Fig. 4A–E show greater R_{11}, R_{22}, P_{12}, and P_{22} coefficients for the Ultra-Flo 145 dialyser® than for the Nephrophan® membrane. On the other hand, the coefficients L_{12}, L_{22}, H_{21}, H_{12}, H_{22}, P_{11}, and P_{21} are greater for the Nephrophan® membrane than for the Ultra-Flo 145 dialyser®.

Taking into account the results of calculations for dependencies $R_{ij} = f(\Delta\pi)_{\Delta P=0}$, $L_{ij} = f(\Delta\pi)_{\Delta P=0}$, $H_{ij} = f(\Delta\pi)_{\Delta P=0}$, and $P_{ij} = f(\Delta\pi)_{\Delta P=0}$ ($i,j \in \{1, 2\}$) (Fig. 3A–D and Fig. 4A–E, and the equations listed in the 2nd column of Table 2), the dependencies ($Q_{Y(Y=R,L,H \text{ or } P)} = f(\Delta\pi)_{\Delta P=0}$ were calculated. The results of calculations are presented in Fig. 5A,B.

The curves presented in Fig. 5 show greater values of the coefficients Q_R, Q_L, Q_H, and Q_P for the Nephrophan® membrane than for the Ultra-Flo 145 dialyser®. Furthermore, the values of coefficients Q_R and Q_L are positive, while

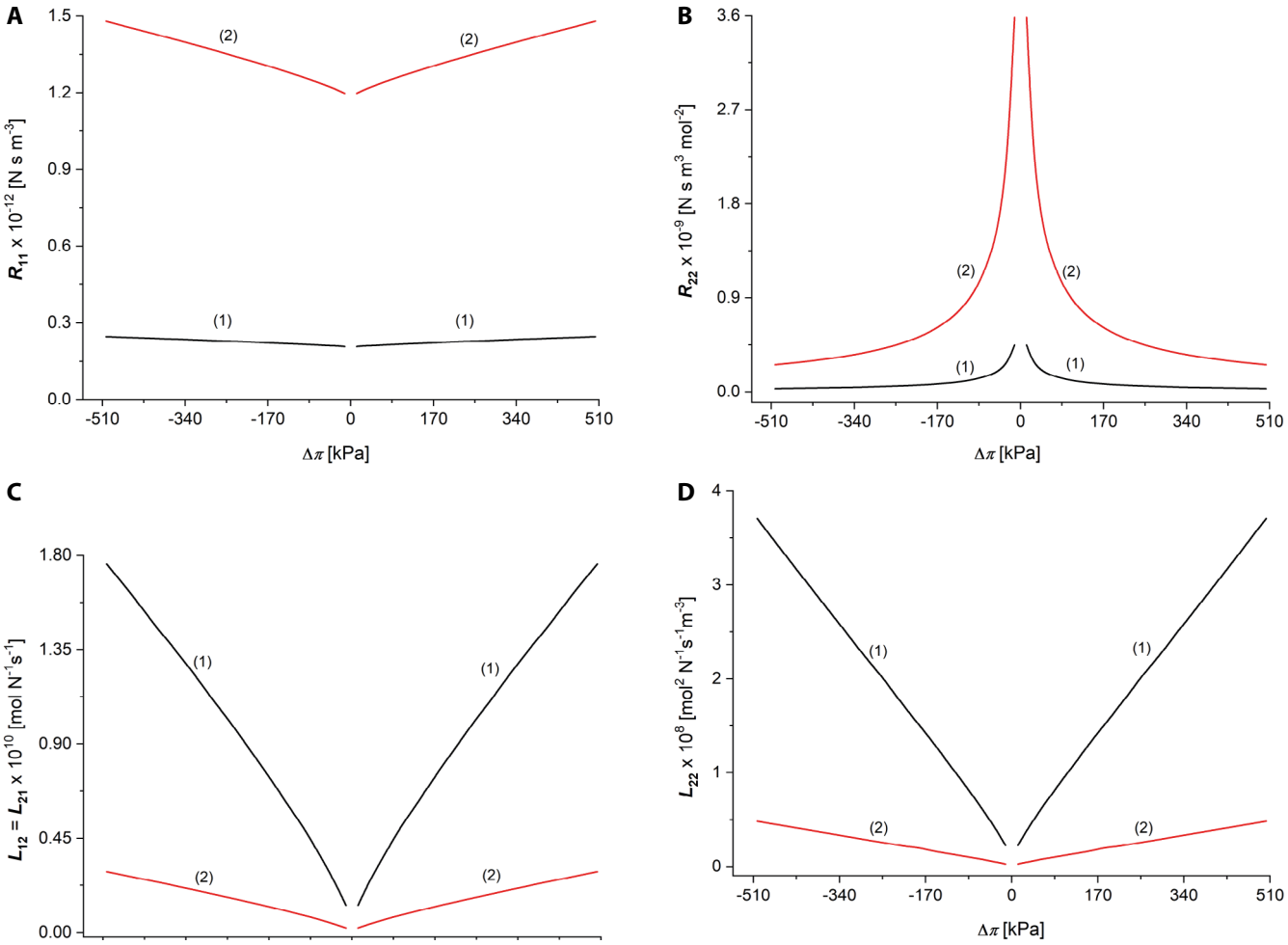

Fig. 3. Illustration of dependencies $R_{ij} = f(\Delta\pi)_{\Delta P=0}$ and $L_{ij} = f(\Delta\pi)_{\Delta P=0}$ ($i,j \in \{1, 2\}$) for aqueous glucose solutions. A. $R_{11} = f(\Delta\pi)_{\Delta P=0}$; B. $R_{22} = f(\Delta\pi)_{\Delta P=0}$; C. $L_{12} = L_{21} = f(\Delta\pi)_{\Delta P=0}$; D. $L_{22} = f(\Delta\pi)_{\Delta P=0}$. Plots marked with (1) were obtained for the Nephrophan® membrane and plots marked with (2) were obtained for the Ultra-Flo 145 dialyser® membrane

Q_H and Q_P are negative. The Nephrophan® membrane fulfilled the relations $Q_R > Q_L$ and $Q_H = Q_P$, while $Q_R = Q_L$ and $Q_H > Q_P$ were fulfilled for the Ultra-Flo 145 dialyser®.

Using the results obtained for dependencies $R_{ij} = f(\Delta\pi)_{\Delta P=0}$, $L_{ij} = f(\Delta\pi)_{\Delta P=0}$, $H_{ij} = f(\Delta\pi)_{\Delta P=0}$, and $P_{ij} = f(\Delta\pi)_{\Delta P=0}$ ($i,j \in \{1, 2\}$) shown in Fig. 3A–D and Fig. 4A–E, as well as $(Q_{Y(Y=R,L,H \text{ or } P)} = f(\Delta\pi)_{\Delta P=0}$, shown in Fig. 5A,B, and the equations listed in the 4th column of Table 2, the dependencies $(e_{max})_{Y(Y=R,L,H \text{ or } P)}$ were calculated. The results of calculations are presented in Fig. 5C,D. The curves in these figures show greater values of the coefficients $(e_{max})_{Y(Y=R,L,H \text{ or } P)}$ for the Nephrophan® membrane than for the Ultra-Flo 145 dialyser® membrane. Also, the coefficients $(e_{max})_{Y(Y=R,L,H \text{ or } P)}$ are positive. For the Nephrophan® membrane, the relations $(e_{max})_R > (e_{max})_L$ and $(e_{max})_H = (e_{max})_P$ are fulfilled. In turn, for the Ultra-Flo 145 dialyser® membrane, $(e_{max})_R = (e_{max})_L = (e_{max})_H < (e_{max})_P$.

Accounting for the results obtained for $R_{ij} = f(\Delta\pi)_{\Delta P=0}$, $L_{ij} = f(\Delta\pi)_{\Delta P=0}$, $H_{ij} = f(\Delta\pi)_{\Delta P=0}$, and $P_{ij} = f(\Delta\pi)_{\Delta P=0}$ ($i,j \in \{1, 2\}$), shown in Fig. 3A–D, Fig. 4A–D and Fig. 5A–C, as well as Equations (10–13), the dependencies $\phi(S)_{Y(Y=R,L,H \text{ or } P)} = f(\Delta\pi)_{\Delta P=0}$, were calculated. The results of calculations are presented in Fig. 6A,B.

The curves presented in Fig. 6A,B show greater values of the coefficients $\phi(S)_{Y(Y=R,L,H \text{ or } P)}$ for Nephrophan® than for the Ultra-Flo 145 dialyser® membrane. These findings indicate that the dissipation of energy is greater in the Nephrophan® membrane than in the Ultra-Flo 145 dialyser® membrane under similar transport conditions. Furthermore, the values of coefficients $\phi(S)_{Y(Y=R,L,H \text{ or } P)}$ are positive, and the relationship $\phi(S)_R > \phi(S)_L > \phi(S)_H > \phi(S)_P$ is true for both the Nephrophan® and Ultra-Flo 145 dialyser® membranes.

Using the results obtained for the dependencies $(e_{max})_{Y(Y=R,L,H \text{ or } P)}$ and $\phi(S)_{Y(Y=R,L,H \text{ or } P)} = f(\Delta\pi)_{\Delta P=0}$, shown in Fig. 5C,D and Fig. 6A,B, respectively, and in Equation (16), the dependencies $\phi(F)_{Y(Y=R,L,H \text{ or } P)} = f(\Delta\pi)_{\Delta P=0}$, were calculated.

The results of the calculations presented in Fig. 6C,D show greater values of the coefficients $\phi(F)_{Y(Y=R,L,H \text{ or } P)}$ for Nephrophan® in comparison to the Ultra-Flo 145 dialyser® membrane. They also show positive values for the coefficients $\phi(F)_{Y(Y=R,L,H \text{ or } P)}$. The relations $\phi(F)_R > \phi(F)_L > \phi(F)_H > \phi(F)_P$ are fulfilled for both the Nephrophan® and Ultra-Flo 145 dialyser® membranes.

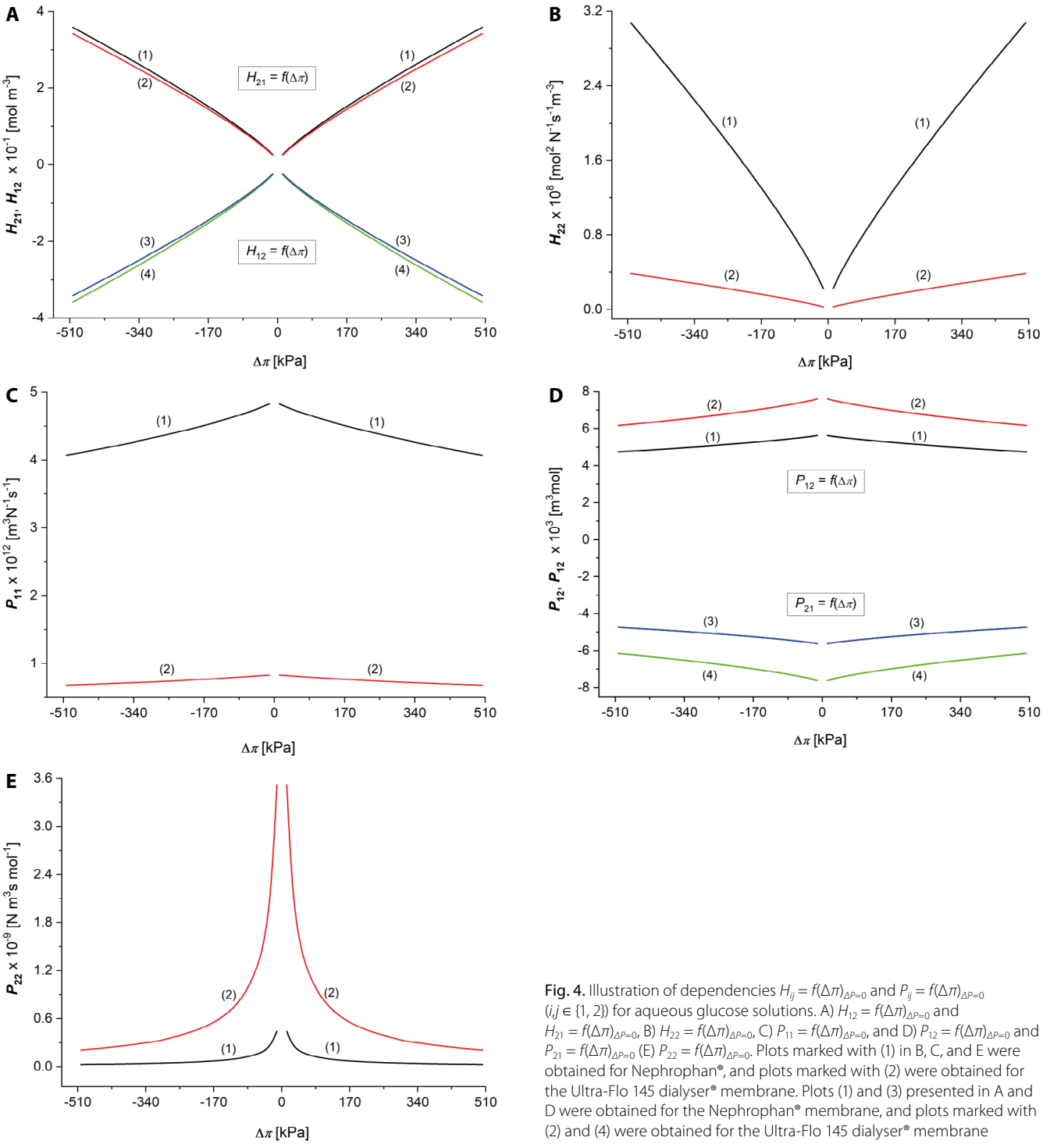

Fig. 4. Illustration of dependencies $H_{ij} = f(\Delta\pi)_{\Delta P=0}$ and $P_{ij} = f(\Delta\pi)_{\Delta P=0}$ ($i,j \in \{1, 2\}$) for aqueous glucose solutions. A) $H_{12} = f(\Delta\pi)_{\Delta P=0}$ and $H_{21} = f(\Delta\pi)_{\Delta P=0}$, B) $H_{22} = f(\Delta\pi)_{\Delta P=0}$, C) $P_{11} = f(\Delta\pi)_{\Delta P=0}$, and D) $P_{12} = f(\Delta\pi)_{\Delta P=0}$ and $P_{21} = f(\Delta\pi)_{\Delta P=0}$ (E) $P_{22} = f(\Delta\pi)_{\Delta P=0}$. Plots marked with (1) in B, C, and E were obtained for Nephrophan®, and plots marked with (2) were obtained for the Ultra-Flo 145 dialyser® membrane. Plots (1) and (3) presented in A and D were obtained for the Nephrophan® membrane, and plots marked with (2) and (4) were obtained for the Ultra-Flo 145 dialyser® membrane

Considering the results obtained for dependences $(e_{max})_{Y(Y=R,L,H \text{ or } P)} = f(\Delta\pi)_{\Delta P=0}$ and $\phi(S)_{Y(Y=R,L,H \text{ or } P)} = f(\Delta\pi)_{\Delta P=0}$), shown in Fig. 5C,D and Fig. 6A,B, respectively, and in Equation (17), the dependencies $\phi(U)_{Y(Y=R,L,H \text{ or } P)} = f(\Delta\pi)_{\Delta P=0}$ were calculated and are shown in Fig. 6E,F.

The curves presented in Fig. 6A–F show greater values of $\phi(U)_{Y(Y=R,L,H \text{ or } P)}$ for the Nephrophan® membrane than the Ultra-Flo 145 dialyser® membrane. Furthermore, $\phi(U)_{Y(Y=R,L,H \text{ or } P)}$ are positive, and the relations $\phi(U)_R > \phi(U)_L > \phi(U)_H > \phi(U)_P$ are fulfilled for both membranes.

Discussion

Using Peusner's lattice thermodynamics formalism, the *R*, *L*, *H*, and *P* versions of the KKP equations are obtained by transforming the classical Kedem–Katchalsky equations.[5] Meanwhile, the equations listed in Table 1 should be considered in order to obtain the *R*, *L*, *H*, and *P* versions of the equations for energy dissipation (*S*-energy).

The characteristics of $\phi(S)_{Y(Y=R,L,H \text{ or } P)} = f(\Delta\pi, \Delta P)$ should have different types of curved surfaces. Indeed, this was

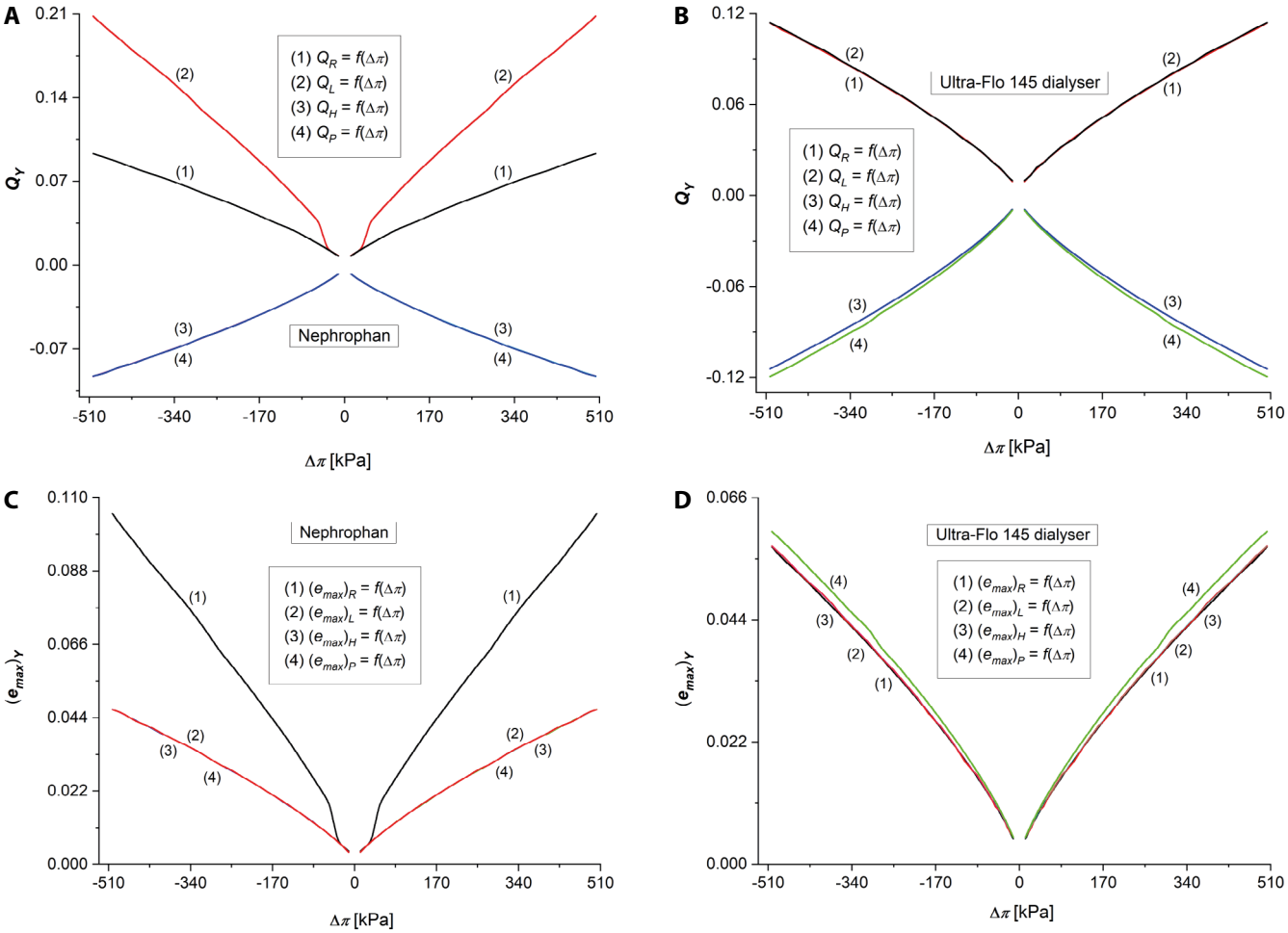

Fig. 5. Illustration of dependencies $Q_{Y\,(Y=R,L,H\,or\,P)} = f(\Delta\pi)_{\Delta P=0}$ and $(e_{max})_{(Y=R,L,H\,or\,P)} = f(\Delta\pi)_{\Delta P=0}$ for aqueous glucose solutions. Plots 1, 2, 3, and 4 shown in A and C were obtained for the Nephrophan® membrane, and plots 1, 2, 3, and 4 in B and D represent the Ultra-Flo 145 dialyser® membrane

previously confirmed by the characteristics of $\phi(S)_L = f(\Delta\pi, \Delta P)$ for a bacterial nanocellulose membrane (Biofill).[8] Similarly, the characteristics of $\phi(S)_{Y\,(Y=R,L,H\,or\,P)} = f(\Delta P, \Delta\pi/\overline{C_s})$ should have different types of curved surfaces, and the characteristics of $\phi(S)_L = f(\Delta P, \Delta\pi/\overline{C_s})$ presented in past work confirm this hypothesis.[7]

As previously mentioned, Equations (6–9) do not contain fluxes J_v and J_s, but contain thermodynamic forces ΔP and $\Delta\pi$. Therefore, these equations constitute the thermodynamic force version of equations for $\phi(S)_{Y\,(Y=R,L,H\,or\,P)}$. As such, a flux version of the equations for $\phi(S)_{Y\,(Y=R,L,H\,or\,P)}$ can also be obtained. For this purpose, thermodynamic forces, $\Delta P - \Delta\pi$ and $\Delta\pi/\overline{C_s}$, should be eliminated from Equation (3) using the equations listed in Table 1. Equations for flux versions of $\phi(S)_{Y\,(Y=R,L,H\,or\,P)}$ have the form (Eq. 22–25):

$$\phi(S)_R = \left[R_{11}J_v^2 + (R_{12} + R_{21})J_vJ_s + R_{22}J_s^2\right] \tag{22}$$

$$\phi(S)_L = \frac{1}{(L_{11}L_{22} - L_{12}L_{21})}\left[L_{22}J_v^2 - (L_{12} + L_{21})J_vJ_s + L_{11}J_s^2\right] \tag{23}$$

$$\phi(S)_H = \frac{1}{H_{22}}\left[(H_{11}H_{22} - H_{12}H_{21})J_v^2 + (H_{12} - H_{21})J_vJ_s + J_s^2\right] \tag{24}$$

$$\phi(S)_P = \frac{1}{P_{11}}\left[J_v^2 + (P_{21} - P_{12})J_vJ_s + P_{12}J_s^2\right] \tag{25}$$

Explicit forms of Peusner coefficients R_{ij}, L_{ij}, H_{ij}, and P_{ij} ($i,j \in \{1, 2\}$) appearing in the above equations is presented in Table 1. The Equations (10–13) are the flux form of the equations for the intensity of the entropy source. Meanwhile, Equations (6–9) will be useful for numerical calculations of the S-energy, and Equations (22–24) can be used for calculations based on experimentally determined J_v and J_s.

Conclusions

Equations describing $\phi(S)_{Y\,(Y=R,L,H\,or\,P)}$ versions of S-energy are the sum of the quadratic equations of the ΔP and $\Delta\pi$ variables. The characteristics of $\phi(S)_{Y\,(Y=R,L,H\,or\,P)} = f(\Delta\pi)_{\Delta P=0}$ are the second-degree curves located in the 1st and 2nd quadrants of the coordinate system.

Characteristics of $\phi(S)_{Y\,(Y=R,L,H\,or\,P)} = f(\Delta\pi)_{\Delta P=0}$, illustrated by curves 1, 2, 3 and 4, for both Nephrophan® and Ultra-Flo 145 dialyser® membranes, have different forms. For the same $\Delta\pi$ values in the Nephrophan® membrane, curves 1, 2, 3, and 4 for the dependencies

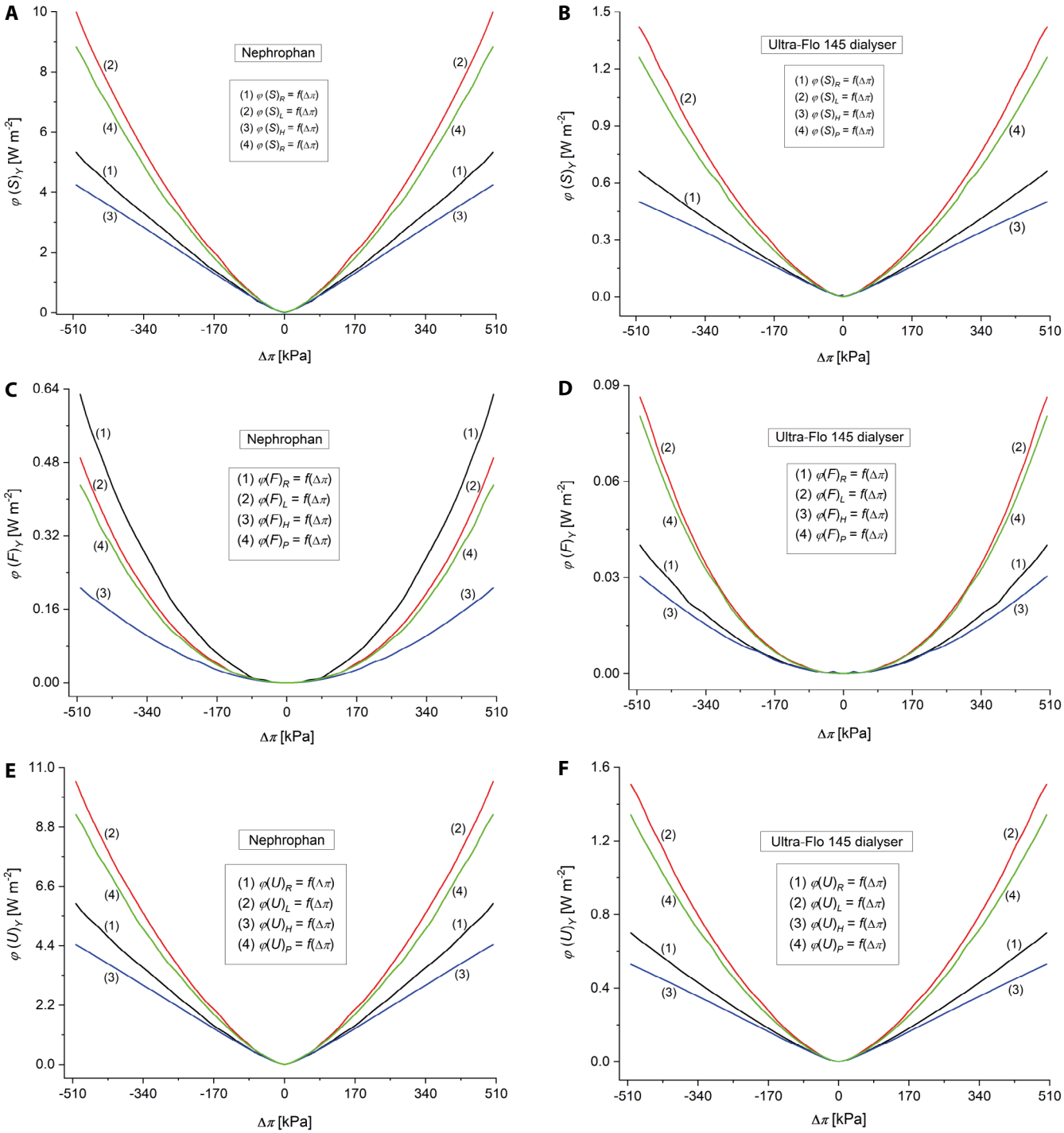

Fig. 6. Illustration of dependencies $\varphi(S)_{Y\,(Y=R,L,H\text{ or }P)} = f(\Delta\pi)_{\Delta P=0}$, $\varphi(F)_{Y\,(Y=R,L,H\text{ or }P)} = f(\Delta\pi)_{\Delta P=0}$, and $\varphi(U)_{Y\,(Y=R,L,H\text{ or }P)} = f(\Delta\pi)_{\Delta P=0}$ for aqueous glucose solutions. Plots 1–4 in A, B, and E were obtained for the Nephrophan membrane, and plots 1–4 in B, D, and F represent the Ultra-Flo 145 dialyser® membrane

$\phi(S)_{Y\,(Y=R,L,H\text{ or }P)} = f(\Delta\pi)_{\Delta P=0}$, $\phi(F)_{Y\,(Y=R,L,H\text{ or }P)} = f(\Delta\pi)_{\Delta P=0}$, and $\phi(U)_{Y\,(Y=R,L,H\text{ or }P)} = f(\Delta\pi)_{\Delta P=0}$, satisfy the following relations: $\phi(S)_L > \phi(S)_P > \phi(S)_R > \phi(S)_H$, $\phi(F)_R > \phi(F)_L > \phi(F)_P > \phi(F)_H$ and $\phi(U)_L > \phi(U)_P > \phi(U)_R > \phi(U)_H$. In contrast, the same $\Delta\pi$ values for the Ultra-Flo 145 dialyser® membrane, curves 1, 2, 3, and 4 for the dependencies $\phi(S)_{Y\,(Y=R,L,H\text{ or }P)} = f(\Delta\pi)_{\Delta P=0}$, $\phi(F)_{Y\,(Y=R,L,H\text{ or }P)} = f(\Delta\pi)_{\Delta P=0}$, and $\phi(U)_{Y\,(Y=R,L,H\text{ or }P)} = f(\Delta\pi)_{\Delta P=0}$, satisfy the following relations, $\phi(S)_L > \phi(S)_P > \phi(S)_R > \phi(S)_H$, $\phi(F)_L > \phi(F)_P > \phi(F)_R > \phi(F)_H$ and $\phi(U)_L > \phi(U)_P > \phi(U)_R > \phi(U)_H$.

ORCID iDs

Andrzej Ślęzak https://orcid.org/0000-0001-6818-2099
Sławomir Marek Grzegorczyn https://orcid.org/0000-0002-5248-3505
Anna Pilis https://orcid.org/0000-0002-5022-6820
Izabella Ślęzak-Prochazka https://orcid.org/0000-0002-0707-2213

References

1. Coveney P, Highfield R. *The Arrow of Time: The Quest to Solve Time's Greatest Mystery*. London, UK: HarperCollins Publishers; 1991. ISBN:978-0-00-654462-3.
2. Kondepudi D. *Introduction to Modern Thermodynamics*. Chichester, UK: Wiley & Sons; 2008. ISBN:978-0-470-98649-3.

3. Demirel Y, Sandler SI. Thermodynamics and bioenergetics. *Biophys Chem*. 2002;97(2–3):87–111. doi:10.1016/S0301-4622(02)00069-8
4. Delmotte M, Chanu J. Non-equilibrium thermodynamics and membrane potential measurement in biology. In: Millazzo G, ed. *Topics in Bioelectrochemistry and Bioenergetics*. Vol. 3. Chichester, UK: Wiley & Sons; 1980:307–359, ISBN:978-0-674-49411-4.
5. Katchalsky A, Curran PF. *Nonequilibrium Thermodynamics in Biophysics*. Harvard, USA: Harvard University Press; 1965. doi:10.4159/harvard.9780674494121
6. Klimek R. Biology of cancer: Thermodynamic answers to some questions. *Neuro Endocrinol Lett*. 2001;22(6):413–416. PMID:11781537.
7. Batko KM, Ślęzak-Prochazka I, Ślęzak A, Bajdur WM, Włodarczyk-Makuła M. Management of energy conversion processes in membrane systems. *Energies*. 2022;15(5):1661. doi:10.3390/en15051661
8. Ślęzak A, Ślęzak-Prochazka I, Grzegorczyn S, Jasik-Ślęzak J. Evaluation of S-entropy production in a single-membrane system in concentration polarization conditions. *Transp Porous Med*. 2017;116(2):941–957. doi:10.1007/s11242-016-0807-7
9. Baker RW. *Membrane Technology and Applications*. 3rd ed. Chichester, UK–Hoboken, USA: John Wiley & Sons; 2012. ISBN:978-1-118-35971-6.
10. Peusner L. *Studies in Network Thermodynamics*. Amsterdam, the Netherlands–New York, USA: Elsevier; 1986. ISBN:978-0-444-42580-5.
11. Batko KM, Slezak-Prochazka I, Grzegorczyn S, Slezak A. Membrane transport in concentration polarization conditions: Network thermodynamics model equations. *J Por Media*. 2014;17(7):573–586. doi:10.1615/JPorMedia.v17.i7.20
12. Batko KM, Ślęzak-Prochazka I, Ślęzak A. Network hybrid form of the Kedem–Katchalsky equations for non-homogenous binary non-electrolyte solutions: Evaluation of P_{ij}* Peusner's tensor coefficients. *Transp Porous Med*. 2015;106(1):1–20. doi:10.1007/s11242-014-0352-1
13. Batko KM, Ślęzak A. Evaluation of the global *S*-entropy production in membrane transport of aqueous solutions of hydrochloric acid and ammonia. *Entropy*. 2020;22(9):1021. doi:10.3390/e22091021
14. Peusner L. Hierarchies of irreversible energy conversion systems. II. Network derivation of linear transport equations. *J Ther Biol*. 1985;115(3):319–335. doi:10.1016/S0022-5193(85)80195-8
15. Ślęzak-Prochazka I, Batko KM, Wąsik S, Ślęzak A. H* Peusner's form of the Kedem–Katchalsky equations for non-homogenous non-electrolyte binary solutions. *Transp Porous Med*. 2016;111(2):457–477. doi:10.1007/s11242-015-0604-8
16. Ślęzak A, Grzegorczyn S, Batko KM. Resistance coefficients of polymer membrane with concentration polarization. *Transp Porous Med*. 2012;95(1):151–170. doi:10.1007/s11242-012-0038-5
17. Batko KM, Ślęzak A, Pilis W. Evaluation of transport properties of biomembranes by means of Peusner network thermodynamics. *Acta Bioeng Biomech*. 2021;23(2):63–72. doi:10.37190/ABB-01774-2020-04
18. Anton-Sales I, D'Antin JC, Fernández-Engroba J, et al. Bacterial nanocellulose as a corneal bandage material: A comparison with amniotic membrane. *Biomater Sci*. 2020;8(10):2921–2930. doi:10.1039/D0BM00083C
19. Batko K, Ślęzak-Prochazka I, Grzegorczyn S, Pilis A, Dolibog P, Ślęzak A. Energy conversion in Textus Bioactiv Ag membrane dressings using Peusner's network thermodynamic descriptions. *Polim Med*. 2022;52(2):57–66. doi:10.17219/pim/153522
20. Harma B, Gül M, Demircan M. The efficacy of five different wound dressings on some histological parameters in children with partial-thickness burns. *J Burn Care Res*. 2020;41(6):1179–1187. doi:10.1093/jbcr/iraa063
21. Ślęzak A. Irreversible thermodynamic model equations of the transport across a horizontally mounted membrane. *Biophys Chem*. 1989;34(2):91–102. doi:10.1016/0301-4622(89)80047-X
22. Dworecki K, Slezak A, Ornal-Wasik B, Wasik S. Effect of hydrodynamic instabilities on solute transport in a membrane system. *J Membrane Sci*. 2005;265(1–2):94–100. doi:10.1016/j.memsci.2005.04.041
23. Ślęzak A. A model equation for the gravielectric effect in electrochemical cells. *Biophys Chem*. 1990;38(3):189–199. doi:10.1016/0301-4622(90)87001-2
24. Ślęzak A, Grzegorczyn S, Jasik-Ślęzak J, Michalska-Małecka K. Natural convection as an asymmetrical factor of the transport through porous membrane. *Transp Porous Med*. 2010;84(3):685–698. doi:10.1007/s11242-010-9534-7
25. Slezak A, Dworecki K, Anderson JE. Gravitational effects on transmembrane flux: The Rayleigh–Taylor convective instability. *J Membrane Sci*. 1985;23(1):71–81. doi:10.1016/S0376-7388(00)83135-X
26. Ślęzak A, Dworecki K, Jasik-Ślęzak J, Wąsik J. Method to determine the critical concentration Rayleigh number in isothermal passive membrane transport processes. *Desalination*. 2004;168:397–412. doi:10.1016/j.desal.2004.07.027
27. Jasik-Ślęzak J, Ślęzak-Prochazka I, Ślęzak A. Evaluation of the Peusner's coefficients matrix for polymeric membrane and ternary non-electrolyte solutions [in Polish]. *Polim Med*. 2014;44(3):167–178. PMID:25696941.
28. Kedem O, Caplan SR. Degree of coupling and its relation to efficiency of energy conversion. *Trans Faraday Soc*. 1965;61:1897. doi:10.1039/tf9656101897
29. Caplan SR. Nonequilibrium thermodynamics and its application to bioenergetics. In: Sanadi RD, ed. *Current Topics in Bioenergetics*. Vol. 4. Elsevier; 1971:1–79. doi:10.1016/B978-0-12-152504-0.50008-3
30. Klinkman H, Holtz M, Willgerodt W, Wilke G, Schoenfelder D. Nephrophan: Eine neue Dialysemembrane. *Zeits Urolog Nephrol*. 1969;4:285–292.
31. Richter T, Keipert S. In vitro permeation studies comparing bovine nasal mucosa, porcine cornea and artificial membrane: Androstenedione in microemulsions and their components. *Eur J Pharm Biopharm*. 2004;58(1):137–143. doi:10.1016/j.ejpb.2004.03.010
32. Twardowski ZJ. History of hemodialyzers' designs. *Hemodialysis Int*. 2008;12(2):173–210. doi:10.1111/j.1542-4758.2008.00253.x